Efficient Thin Polymer Coating as a Selective Thermal Emitter for Passive Daytime Radiative Cooling

Udayan Banik, Ashutosh Agrawal†, Hosni Meddeb, Oleg Sergeev, Nies Reininghaus, Maximilian Götz-Köhler, Kai Gehrke, Jonas Stührenberg, Martin Vehse, Maciej Sznajder§ζ, Carsten Agert.*

DLR Institute of Networked Energy Systems, 26129 Oldenburg, Germany

§ DLR Institute of Space Systems, 28359 Bremen, Germany

ζ University of Bremen, MAPEX Center for Materials and Processes, 28359 Bremen, Germany

KEYWORDS: sub ambient radiative cooler, organopolysilazane, polymer derived coating, thin photonic emitter, silicon oxycarbonitride emitter

ABSTRACT: Radiative cooling to sub ambient temperatures can be efficiently achieved through spectrally selective emission, which until now has only been realized using complex nanoengineered structures. Here, a simple dip coated planar polymer emitter derived from polysilazane, which exhibits strong selective emissivity in the atmospheric transparency window of 8-13 μm is demonstrated. The 5 μm thin silicon oxycarbonitride coating has an emissivity of 0.86 in this spectral range, owing to alignment of the frequencies of bond vibrations arising from the polymer. Furthermore, atmospheric heat absorption is suppressed due to its low emissivity outside the atmospheric transparency window. The reported structure with the highly transparent polymer and underlying silver mirror reflects 97% of the incoming solar irradiation. A temperature reduction of 6.8 °C below ambient was achieved by the structure under direct sunlight, yielding a cooling power of 93.7 Wm^{-2}. The structural simplicity, durability, easy applicability and high selectivity make polysilazane a unique emitter for efficient prospective passive daytime radiative cooling structures.

INTRODUCTION

Conventional cooling systems accounted for 8.5% of the total final electricity consumption and contributed to 1 Gt of CO_2 emissions worldwide in 2019.[1] Demands for conventional air conditioning are set to soar in hotter regions due to rising temperatures and is expected to exacerbate the greenhouse effect.[2] Although, powering conventional air conditioners with renewables can reduce CO_2 emissions, noise emissions from condenser units and their contribution to the heat island effect will pose challenges in urbanized areas.[3,4] Passive radiative cooling technology offers substantial advantages over active cooling methods due to their ability to operate without or with nominal electricity requirements.[5,6] The system exploits the transparency of the atmosphere in the mid Infrared (MIR) wavelength of 8-13 μm to expel heat from an object to space by radiative heat transfer using the temperature difference between earth at ~300 K and space at ~3 K. Although cooling demands mostly peak during daytime, most conventional radiative cooling strategies were found to be satisfactory only for nighttime applications in absence of solar heating.[7–10] Recently, passive daytime radiative cooling (PDRC) was realized by suppression of solar heating using photonic structures, which has substantially increased the research interest in the field of passive daytime cooling technology.[11] An efficient PDRC strategy presents a promising, yet elegant but environmentally green and sustainable alternative to conventional active cooling systems for buildings.

A prerequisite to achieve passive radiative cooling during daytime is that a structure should strongly reflect incoming solar irradiation in between 0.3-2.5 μm and simultaneously emit through the atmospheric transparency spectral window of 8-13 μm. The emissive layers for the daytime radiative cooling structures can be categorized into either broadband or spectrally selective emitters.[10] Broadband emitters are characterized by high emissivity in the MIR range and therefore

have high radiative power throughput compared to the spectrally selective counterparts.[5] The intrinsic high emissivity of the polymer emitters arise from the molecular vibration modes of functional groups of the polymeric bonds that fits to the atmospheric transparency window wavelength range.[12] Typically, 20-200 μm thick polymer films are required to achieve high emissivity from the bulk material in the MIR region for a bi-layer structure.[13–16] While both carbon based[12,17–20] and silicon based[13,21,22] polymers have been extensively investigated to make PDRC structures, a drawback of broadband emissive polymer materials is that thick polymer layers generally have undesired absorption due to inadequate transparency in the solar spectral range.[16,23] Additionally, due to the broadband absorption characteristic in the MIR region, polymer emitters absorb heat from the atmosphere and surrounding objects, limiting the sub ambient cooling performance during the daytime. [6,24,25]

Sub ambient cooling can be efficiently achieved by spectrally selective emitters that have high emissivity in the 8-13 μm spectral range and low IR absorption outside of this window. This ensures low atmospheric heat absorption at other wavelengths in MIR where the atmosphere does not allow transmission.[26] Spectrally selective emitter structures are generally designed using nanophotonic approaches to achieve high emissivity in between 8-13 μm. This can be realized by modulating the emissivity spectra using Fabry-Pérot interferences[5], multi-layer photonic crystals[11,27–29], nanofibers[30], grating patterns[31,32] or embedded microspheres.[33] All of these concepts implicate fabrication on nanometer precision and notable manufacturing complexity for larger scale production.[5,26,34] Contrastingly, polymer based radiative cooling devices can be produced using cost-effective, industry compatible and scalable manufacturing techniques[14,20] but a planar polymer PDRC structure exhibiting spectrally selective properties has not been reported yet.

In this paper, we demonstrate for the first time a spectrally selective planar polymer emitter derived from Polysilazane which was used in combination with a highly reflective 230 nm thick silver layer on an aluminum substrate to create a PDRC structure. Polysilazanes are silicon-based precursor polymers with alternating silicon and nitrogen atoms[35] in its backbone and have been an area of intense research since the 1960's.[35,36] Substantial efforts were made to understand the optical properties of PSZ coatings.[37–41] Recently we identified and demonstrated the high emissivity, optical transparency, flexibility, and protective properties against mechanical abrasion of silicon oxycarbonitride (SiCNO) emitter coating derived from PSZ on thin-film solar cells for space applications.[37,42] PSZ derived coatings show outstanding mechanical sturdiness, hydrophobicity, chemical stability and have strong adhesive properties to most substrates even as cross-linked polymers.[43–45] These desirable properties of the PSZ polymer coating make it an appealing material to be used as an emitter for PDRC applications. The thin polymer emitter layer, fabricated from a polysilazane (PSZ) precursor is easy to apply and has molecular vibrations that overlap with the 8-13 μm atmospheric transmission window exceedingly well. Using a simple setup, we experimentally measured a maximum temperature drop of 6.8 °C below ambient and an average drop of 5 °C by the aforesaid PDRC structure, corresponding to a cooling power of 93.7 Wm^{-2}. We illustrate the relevant properties of the PDRC structure with the SiCNO spectrally selective emitter in the following sections.

RESULTS AND DISCUSSION

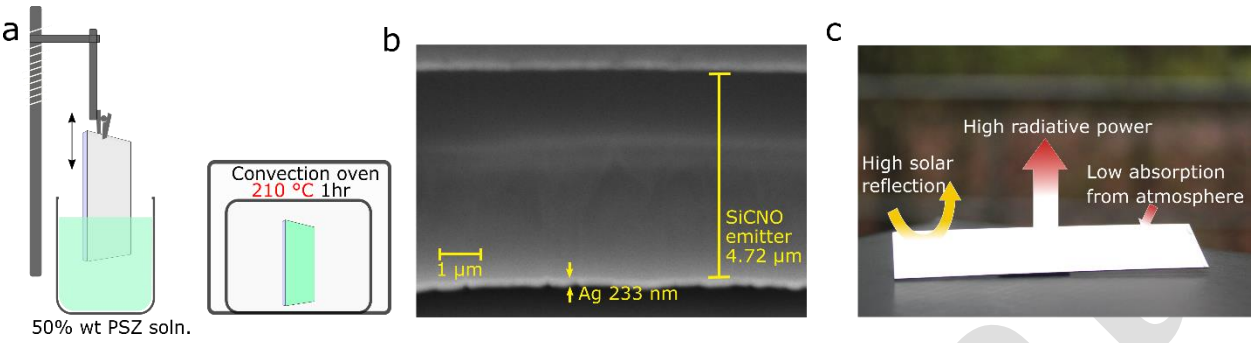

Figure 1. Fabrication and structure of polysilazane polymer coating. a) Schematics showing the dip coating process of the polymer layer on silver coated aluminum substrate. The sample was introduced and hoisted from the solution at a speed of 8.3 mms^{-1}. The wet coating was cured at 210 °C for 1hour while hanging; b) SEM image of the FIB cross section showing the thickness of the SiCNO emitter layer (4.72 µm) and silver back reflector (233 nm); c) a photograph of the SiCNO coated PDRC structure illustrating its properties of high solar reflection (0.3-2.5 µm), high radiative power (8-13 µm) and suppressed downward thermal absorption from atmosphere.

For fabricating the PDRC structure, we applied the PSZ emitter layer on a silver coated aluminum substrate with a simple dip coating process, as illustrated in Figure 1a (see Experimental Section for details). The wet coating transforms into a hardened 3D network of crosslinked polymer when cured at temperatures below 400 °C.[35,36] To prevent spalling and damage to the substrate and the silver mirror the curing was performed at 210 °C in air. The cross section of the bi-layer PDRC structure was studied and is shown in Figure 1b, where the thickness of the emitter and silver reflector was measured to be 4.7 µm and 233 nm respectively. A root-mean square surface roughness (RMS) of about 22.8 nm was determined by AFM investigation (see Supplementary Figure S1). These results confirm the planar surface morphology of the SiCNO

emitter layer. The propitious optical properties of the spectrally selective PDRC structure are demonstrated in Figure 1c. The structure exhibits high solar reflectivity, high radiative power throughput and low IR absorption from atmosphere due to the inherent selective emissivity of the coating. Each feature is comprehensively studied further.

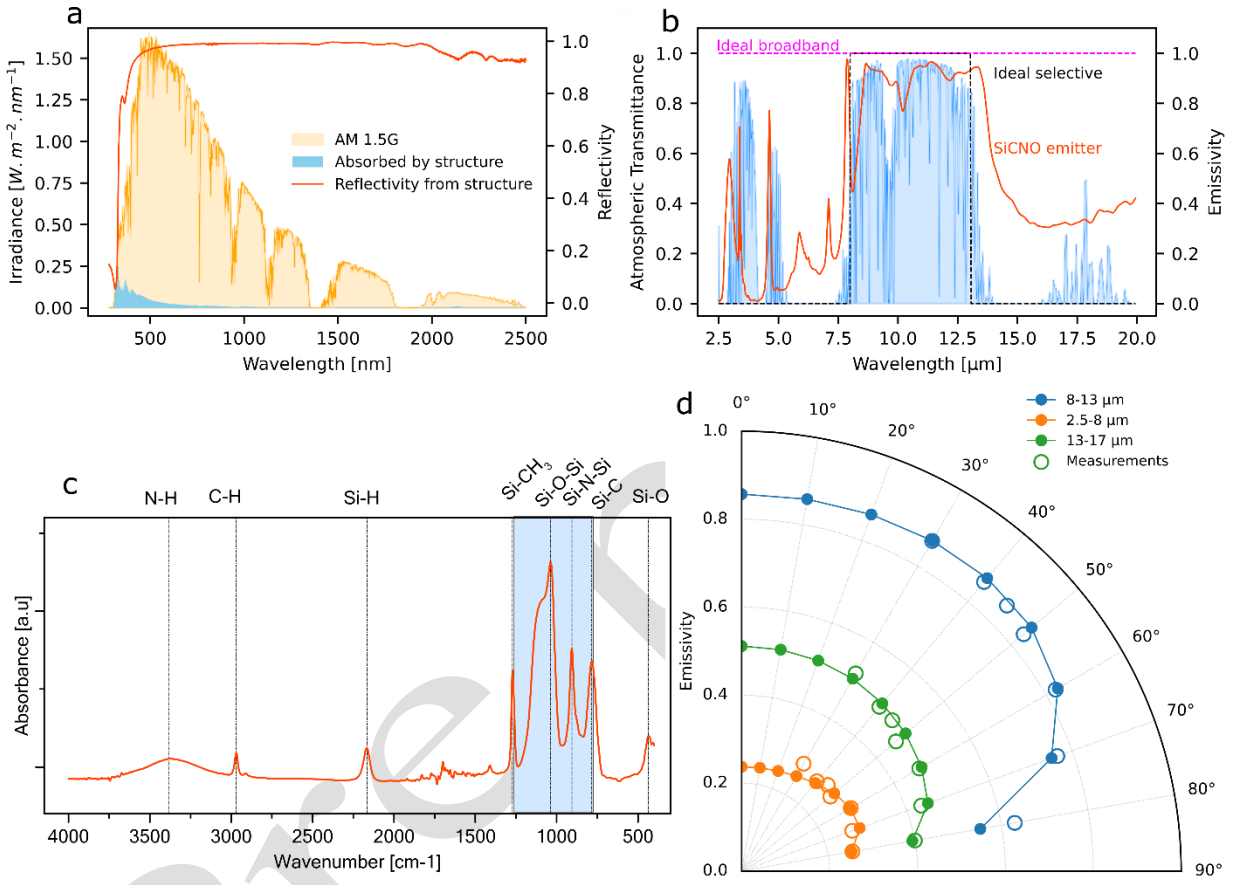

Figure 2. Optical properties of the PDRC structure in the UV-VIS-NIR-MIR range. a) Reflection measurement from the SiCNO coated PDRC structure (in red). The blue shaded part represents the power absorbed by the structure under AM1.5G irradiance (orange shade); b) Emissivity of the PDRC structure (orange) as compared to an ideal selective emitter (dashed black) and ideal broadband emitter (dashed pink) along with atmospheric transmittance (shaded blue). The atmospheric transmittance spectrum at zenith was generated using ATRAN software for mid latitude summer; c) FTIR measurement (absorbance mode) from a PSZ coated silicon wafer for

identification of the resonance bonds. The blue shaded region equates to the primary atmospheric window range of 8-13 μm; d) Modeled angular dependence of emissivity (filled circles) divided into specific wavelength ranges along with measured emissivity (unfilled circles, categorized by color) from the PDRC structure is shown here to demonstrate spectral selectivity.

The measured optical properties of the PDRC structure from the UV-Vis to MIR spectral range is presented in Figure 2. It can be clearly seen from Figure 2a that the reflection of light in between 0.3 to 2.5 μm from the Ag-backed PSZ polymer structure is very high. This is beneficial to ensure minimum heat absorption from the Sun, as 96.9% of the incident light is reflected by the structure (see Equation 1 of Supplementary Text S1). The similarity in reflectance between bare silver reflector and the PSZ coated silver reflector reveals the high transmittance of the cured PSZ polymer in 0.3-2.5 μm wavelength range (see Supplementary Figure S2). The emissivity spectrum of the structure in between 2.5 to 20 μm, measured with a gold integrating sphere is shown in Figure 2b together with the generated atmospheric transmittance spectra from the ATRAN model.[46] All subsequent analysis was carried out with this atmospheric data. The emissivity curve from the structure fits well to the desired wavelength selectivity of an ideal selective emitter, which has ε=1 in between 8-13 μm and ε=0 below 8 μm and above 13 μm (dashed black line in Figure 2b).

The cause of high emissivity of the SiCNO emitter can be explained by vibrational bond analysis as shown in the FTIR spectra of a coated silicon wafer in absorbance mode (Figure 2c). The major vibrational peaks from the FTIR spectra of the polymer coating were identified and the atmospheric spectral transmission window is marked in blue. The peaks at ~3382 cm^{-1}, ~2970 cm^{-1}, ~2166 cm^{-1} are associated to N-H stretching, C-H symmetric stretching and Si-H asymmetric stretching respectively.[43,45]. They are also known as the reactive species since they take part in the

crosslinking reaction during thermal curing. The peak at 1272 cm^{-1} represents the corresponding bending vibrations of Si-CH_3 which is the non-hydrolysable group of polysilazane that does not take part in the crosslinking reaction.[47] The peak around ~436 cm^{-1} originates from the Si-O rocking vibrations.[37] The fingerprint region (1500-600cm^{-1}) includes the vibration of the functional groups, which also happens to coincide with the atmospheric transmittance window. The relative broad peak system seen in between 1180-970 cm^{-1} with the prominent peak at ~1038 cm^{-1} is from the Si-O-Si asymmetric stretching, whereas the peaks at ~906 cm^{-1} and ~784 cm^{-1} stems from the Si-N-Si stretching and Si-C stretching in the oligosilsesquioxane network, have their vibrational frequency within the primary atmospheric window (highlighted in blue).[43,47] This allows efficient heat emission by the structure into space without being absorbed by the atmosphere.[12] The spectral selectivity of the SiCNO emitter is illustrated in Figure 2d, by splitting the emissivity into 3 wavelengths ranges. The emissivity for each range was calculated using Equation (1)

$$\varepsilon_{\lambda_1-\lambda_2} = \frac{\int_{\lambda_1}^{\lambda_2}\left(1\text{-}R(\lambda)\right).I_{BB}(T,\lambda)d\lambda}{\int_{\lambda_1}^{\lambda_2} I_{BB}(T,\lambda)d\lambda} \quad (1)$$

where, λ_1 and λ_2 are the limits of the wavelength range under study, $R(\lambda)$ is the reflection spectra and $I_{BB}(\lambda)$ is the spectral irradiance of a blackbody at a temperature of T=300 K. The angular emissivity from the modeled spectra is in good accordance with the measured angular emissivity as can be seen from the overlapping of the filled and unfilled circles. The first spectral range of 8-13 μm denotes the atmospheric window where an emitter should have ideally ε=1 at all angles. In this range the polymer emitter has ε of 0.86 at zenith. In the second spectral range of 2.5-8 μm, the SiCNO emitter exhibits low emissivity of only 0.23, whereas in the third spectral range of 13-17 μm the emitter has emissivity of 0.51 at zenith. An ideal emitter would have ε=0 in both 2.5-8 μm and 13-17 μm as emission is not desired outside the atmospheric transparency window. The

emissivity of the PDRC structure is highest at the surface normal and starts decreasing significantly after 60° (Figure 2d). This compliments well when the emitter is laid horizontally facing the sky as the atmosphere is most transparent at the zenith and least at horizon. Having analyzed the optical properties of the PDRC structure, we conducted an outdoor experiment to verify the passive cooling behavior of the structure.

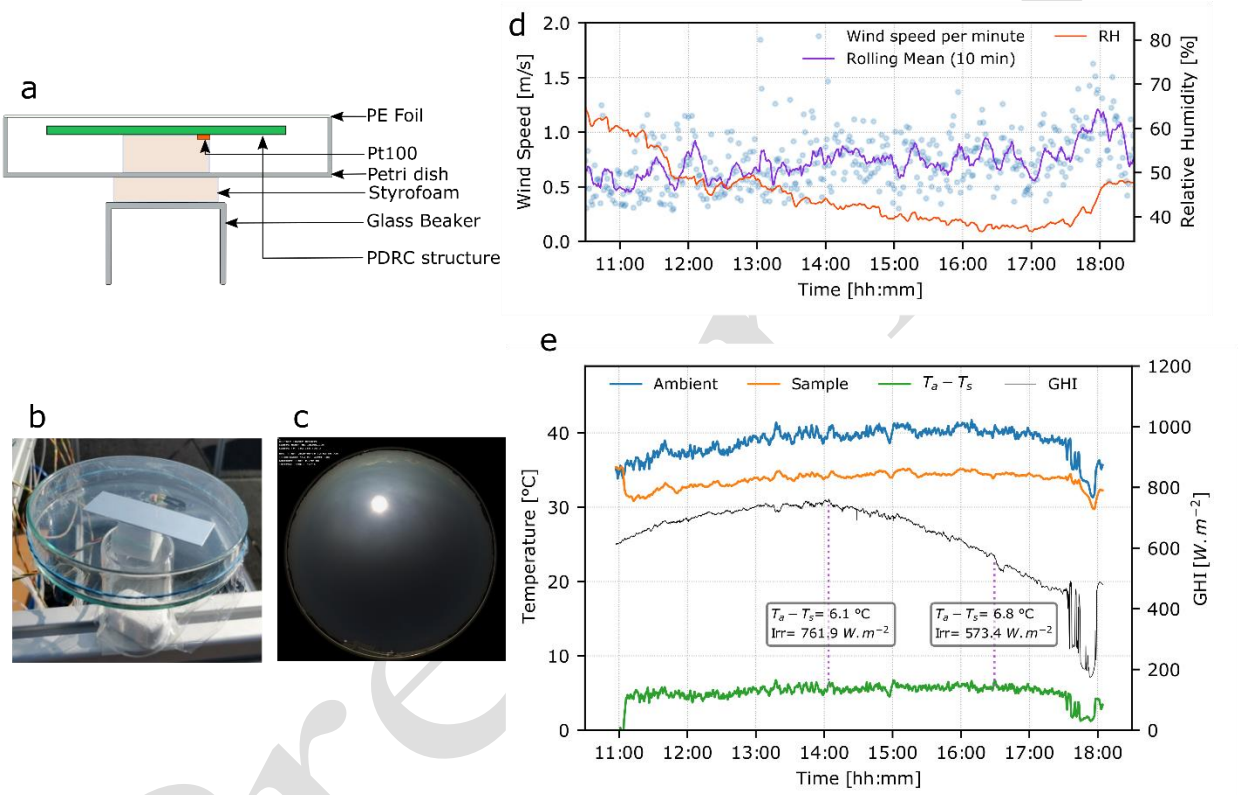

Figure 3. Outdoor experiment showing the cooling performance. a) Schematic of the experimental setup showing the petri dish enclosure; b) A photograph of the sample inside the petri dish enclosure as was taken on the day of experiment; c) Sky camera image from the meteorological station next to the experiment (at the time of highest irradiance, 14:03 hrs.) demonstrating a clear sky; d) Plot showing wind speed measurements and relative humidity during the experiment time; e) Plot showing temperature measurements from the experiment along with measured global

horizontal irradiance and relative humidity. The time of highest GHI and highest temperature drop (Ta-Ts, Ta= ambient, Ts=sample) are annotated and marked with purple dotted lines.

The outdoor rooftop experiment was performed on a hot summer day with clear sky conditions in Oldenburg, Germany (N53°09'05.1" E8°10'01.1"). A petri dish, covered by a polyethylene foil was used as an enclosure (Figure 3a), to reduce the convection losses. Based on previous studies with similar experimental setups, we assumed the value of thermal co-efficient for the parasitic non radiative contribution (h_c) to be 10 $Wm^{-2}K^{-1}$.[15,27,48] Strategically placed Pt100 sensors were used to measure the inner ambient temperature of the enclosure and the sample temperature (see Experimental Section for details). During the experiment the effect of wind remained negligible as can be verified from the wind velocity measurement plot in Figure 3d. The smooth global horizontal irradiance (GHI) curve (black line in Figure 3e) in between 11:00 hrs. and 17:30 hrs. (local time) is indicative of a clear sky. The petri dish setup was temporarily covered with a piece of aluminum foil before it was opened to view the sky. The steep drop in the temperature of the structure below the ambient temperature, on exposure to sky, is a proof of its radiative cooling properties. The device performed steadily throughout the day and an average temperature drop of 5 °C was observed throughout the experimental period. Even with the GHI reaching its peak of 761 Wm^{-2} around 14:03 hrs. the sample was 6 °C colder than the ambient temperature. A maximum drop of 6.8 °C at 16:29 hrs. was achieved. The dependence of radiative cooling on the relative humidity of the surrounding air can also be observed from the rooftop experiment. The maximum temperature drop coincides with the period of the day with low relative humidity i.e., less than 40 %. Around 17:30 hrs. the wind-speed increased and clouds started to appear which resulted in fluctuation of the GHI and an increase of the relative humidity. Presumably, with interferences from the clouds, the atmospheric transmittance window was suppressed resulting in a decrease in

the difference between ambient and the sample temperature. In the following section, we analyze the cooling capability of the prepared structure using an analytical model.

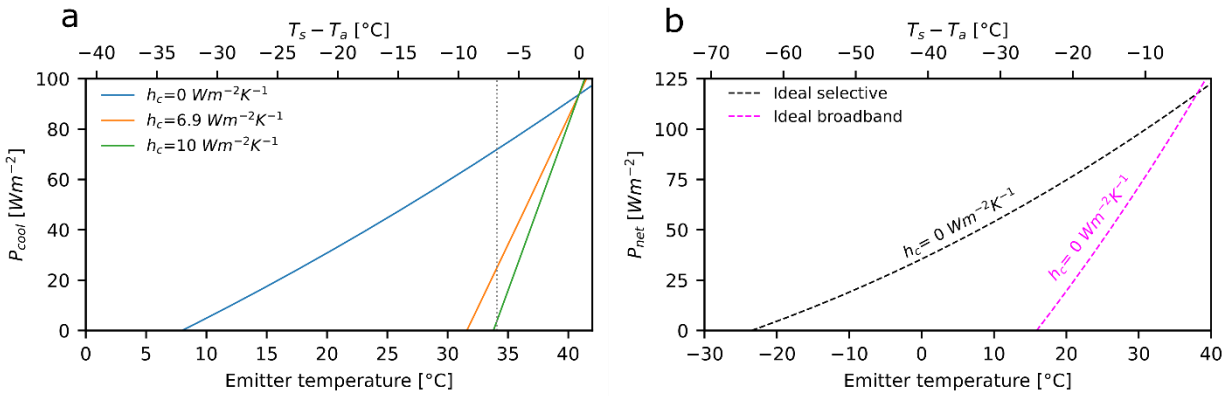

Figure 4. Cooling power analysis. a) Analysis of the cooling power from a SiCNO PDRC structure. The grey dashed line denotes the highest temperature drop of 6.8 °C seen during the outdoor experiment; b) Analysis showing net emissive power versus emitter temperature of different theoretical blackbodies.

A structure exposed to the Sun and sky during the day experiences multiple heat exchanges with the surrounding environment. The net cooling power (P_{cool}) from the structure can be calculated if all individual energy flows are known using the following formula. [11]

$$P_{cool}(T) = P_{rad}(T_{cooler}) - P_{sun} - P_{atm} - P_{cond+conv} \quad (2)$$

Where, P_{rad}, P_{sun}, P_{atm}, $P_{cond+conv}$ is the radiative power throughput from the structure, the absorbed solar irradiance, the absorbed power from the environment in MIR and parasitic heat loss due to the conduction and convection to the environment respectively. Having analyzed each component (see Supplementary Text S1) of the energy balance equation (Equation (2)) we can then determine the cooling power and therefore the efficacy of the structure. The measured ambient temperature at 16:29 hrs, where the highest temperature drop was recorded, was used for the analysis. The cooling potential of the above described PDRC structure is studied in Figure 4a. The maximum

cooling power, or the power at which T_s-T_a=0, was calculated to be 93.7 Wm^{-2}. The intersection of the h_c lines with the axis P_{cool}=0, determines the lowest achievable equilibrium temperature for the emitter. With h_c= 10 $Wm^{-2}K^{-1}$ we arrive at an equilibrium point which is close to 6.8 °C (marked in dotted lines), which validates our analytical model to the experimental results. While a direct comparison of our results with published literature is inadequate due to different experimental conditions, the model predicts an equilibrium temperature of 9.5°C could be achieved with previously published experimental enclosure designs (with h_c= 6.9 $Wm^{-2}K^{-1}$).[11,27] The influence of the parasitic heat losses and enclosure design on the emitter temperature becomes conspicuous as the equilibrium temperature decreases significantly with lower h_c values. With a vacuum enclosure ($h_c \rightarrow 0$ $Wm^{-2}K^{-1}$), the model predicts that the PDRC structure can cool down to around 33 °C below ambient. The net cooling power ($P_{cool} - P_{cond+conv} - P_{sun}$) of the ideal selective and ideal broadband blackbody is shown in Figure 4b for comparison. For the theoretical blackbodies, P_{sun} was assumed to be zero. It is worth mentioning that under vacuum, an ideal selective emitter can reach a minimum temperature (equilibrium point around 64 °C below ambient) much lower than a broadband blackbody (equilibrium point around 25 °C below ambient) even though the net cooling power of the ideal broadband emitter is higher.

The experiments demonstrated here show that a polysilazane based passive daytime cooling structure can combine the cost effectiveness of polymer coatings with good spectral selectivity, that has until now only been achieved using complex structures. A highlight of the PSZ emitter layer is that the vibrations from the functional groups in the fingerprint region coincides precisely (Figure 2c) with the atmospheric window (8-13 µm) making it an ideal selective polymer emitter for PDRC. The 5 µm planar SiCNO emitter, has high emissivity of 0.86 in between 8-13 µm due to the vibration modes from the Si-O-Si, Si-N-Si and Si-C bonds originating from the polymer

network. Therefore it is able to efficiently emit heat into space without being absorbed by the atmosphere and fits the emitter criteria for PDRC strcuture.[12] As the polymer emitter layer in our structure is orders of magnitude thinner than previous reported polymer based PDRC structures, the intrinsic absorption outside the fingerprint region is small.[13,14,20] This is beneficial since we can avoid radiation exchange and therefore minimize the heating between the sample and the atmosphere and surrounding objects in the MIR range. It allows the structure to reach a thermal equilibrium which is below ambient temperature as justified by the cooling power analysis.[6] This further confirms the hypothesis that a selective emitter would be better suited for sub ambient and even sub-freezing temperatures since the end equilibrium temperature is of vital interest.[49] Implicitly, this initial study with PSZ emitter also indicates towards better enclosure designs and finding substitute reflector materials for significantly improved cooling performances and cost-competitiveness.

CONCLUSION

In conclusion, we demonstrate for the first time a passive daytime radiative cooler with a spectrally selective silicon oxycarbonitride emitter derived from polysilazane precursor polymer. A simple bi-layer structure with silver as back reflector and the thin SiCNO emitter layer was designed. Unlike other broadband polymer emitters, the SiCNO coating exhibits low emissivity outside the atmospheric transparency window resulting in a reduced atmospheric absorption, providing the required selective emission for sub-ambient cooling. The high transparency of the polymer layer in the solar spectrum of 0.3-2.5 μm allows reflection of 97% from the PDRC structure, which drastically reduces the solar heat absorption. In an outdoor experiment, we observed a reduction of the sample temperature by 6.8 °C below ambient under direct solar irradiation, corresponding to a cooling power of 93.7 Wm^{-2} from the structure and confirming the

outstanding cooling performance in compliance to the remarkable optical properties of the PSZ emitter layer. This simple bi-layer structure with the thin planar emitter and easy application process, can eliminate the complex fabrication approaches required to achieve spectral selective emission. We anticipate that polysilazane derived coatings will play an important role in residential and industrial cooling applications due to simplicity of the structure, its tenability and industrial scalability.

EXPERIMENTAL SECTION

Sample preparation: A silver layer of 230 nm was deposited by electron beam evaporation (DREVA LAB 450, VTD) on 4 mm thick polished Aluminum plates procured from Alanod GmbH &Co. Kg, Germany. Durazane 1800 purchased from Merck KGaA, Germany was used as precursor and Di-n-butyl ether procured from Fisher Scientific GmbH, Germany was used as the solvent. A solution was prepared by mixing Durazane 1800 (50 wt.%) and di-n-butyl ether (50 wt.%) in a glass flask. The solution was then transferred into a closed glass bottle and kept in a magnetic stirrer with a stir bar for mixing overnight at room temperature. The precursor solution was left standing for 10 minutes in a beaker while covered with a petri dish, in order to remove the bubbles that arose while pouring the solution from the bottle. The samples were cleaned with pressurized air to remove any visible particulates sticking on the surface. Dip coating was carried out under a fume hood at room temperature using an in-house built variable speed dip coater machine. The 2.5 cm x 10 cm substrates were vertically inserted and hoisted out from the solution at a speed of 8.3 mms^{-1} and cured for 1 hour at 210 °C while hanging. The samples were set aside to cool down naturally (see Supplementary Figure S3 for coating on a flexible substrate). A polished silicon wafer was coated similarly to study the bond evolution in the coating.

Characterization: A focused ion beam (FIB) was used to create a cross-section of the structure. The thickness was measured with a Zeiss scanning electron microscope (SEM). The reflectivity of the samples in the solar spectrum of 250 nm to 2500 nm was measured using an Agilent Cary 5000 spectrometer with an integrating sphere. A Brucker Vertex 80V FTIR spectrometer with a gold integrating sphere was used to measure the reflectivity of the sample in the MIR range of 2.5 μm to 20 μm. Angular reflection of the sample in the MIR range between 2.5 μm and 20 μm was measured in between 30°-80° using a VeeMAX II accessory from Pike Technology in a separate PerkinElmer Spectrum 400 FTIR spectrometer. A gold reference was used as a standard.

Optical and Analytical Modeling: An optical model of the PDRC structure was prepared in the Coating Designer (Scout/CODE) software by W. Theiss using experimental measurements. Refractive index data of Ag from the included optical constant database was used.[50] The insulating polysilazane emitter layer was modeled with extended harmonic oscillators representing the bond vibrations in the IR region as suggested by the Model selection criteria for CODE.[51] The modeled reflection spectra were then fitted to experimental spectra where the individual oscillator strength, frequency and damping were adjusted forming a feedback loop (see Supplementary Figure S4 for modelled emissivity spectra). The analytical model to determine the cooling power was prepared in python with suggestions taken from wptherml package and the graphs demonstrated were prepared using matplotlib and Origin 9.1.[52]

Outdoor experiment setup: A simple glass petri dish enclosure with thin polyethylene film of 13 μm thickness as convective barrier and Styrofoam insulators were used to carry out the outdoor experiment. Calibrated class A Pt100 sensors with 4 wire configurations were used to record the temperature. An Agilent 34972A LXI data acquisition unit connected to a laptop was used to monitor the temperature every 5 seconds. The enclosure was placed horizontally facing the sky on

an inverted glass beaker, without any shading or beaming attachments. The measurements were carried out on the rooftop of German Aerospace Center (DLR), Institute of Networked Energy System (N53°09'05.1" E8°10'01.1") on 10.08.2020. See Supplementary Figure S5 for nighttime performance on a winter day. The RH and wind speed were collected from DLR's permanent weather station 136m away from the place of experiment, whereas GHI was measured from another station situated 400m away.

ASSOCIATED CONTENT

Supporting Information.

The following files are available free of charge.

Supplementary Information (PDF)

AUTHOR INFORMATION

Corresponding Author

*Udayan Banik- DLR Institute of Networked Energy Systems, Urban and Residential Technologies, 26129 Oldenburg, Germany, http://orcid.org/0000-0003-2605-2215 E-mail: udayan.banik@dlr.de

Authors

Ashutosh Agrawal- †DLR Institute of Engineering Thermodynamics, Electrochemical Energy Technology, 70569 Stuttgart, Germany, https://orcid.org/0000-0002-3277-5041

Hosni Meddeb- DLR Institute of Networked Energy Systems, Urban and Residential Technologies, 26129 Oldenburg, Germany, https://orcid.org/0000-0001-8939-7910

Oleg Sergeev- DLR Institute of Networked Energy Systems, Urban and Residential Technologies, 26129 Oldenburg, Germany, https://orcid.org/0000-0002-5022-6118

Nies Reininghaus- DLR Institute of Networked Energy Systems, Urban and Residential Technologies, 26129 Oldenburg, Germany, https://orcid.org/0000-0002-9509-274X

Maximilian Götz-Köhler- DLR Institute of Networked Energy Systems, Urban and Residential Technologies, 26129 Oldenburg, Germany, http://orcid.org/0000-0002-6078-4359

Kai Gehrke- DLR Institute of Networked Energy Systems, Urban and Residential Technologies, 26129 Oldenburg, Germany, https://orcid.org/0000-0002-0591-8289

Jonas Stührenberg- DLR Institute of Networked Energy Systems, Energy System Analysis, 26129 Oldenburg, Germany, https://orcid.org/0000-0002-3777-2632

Martin Vehse- DLR Institute of Networked Energy Systems, Urban and Residential Technologies, 26129 Oldenburg, Germany, https://orcid.org/0000-0003-0578-6121

Maciej Sznajder- DLR Institute of Space Systems, Mechanics and Thermal Systems, 28359 Bremen, Germany.

University of Bremen, MAPEX Center for Materials and Processes, 28359 Bremen, Germany
https://orcid.org/0000-0002-9917-0581

Carsten Agert- DLR Institute of Networked Energy Systems, 26129 Oldenburg, Germany, https://orcid.org/0000-0003-4733-5257

Funding Sources

None

Conflict of Interest Statement

A patent (DE 10 2020 134 437.6) has been filed on the work described here by authors U. Banik, H. Meddeb, O. Sergeev and K. Gehrke.

ACKNOWLEDGMENT

The authors thank Jens Sürig Morieng for his help with building the dip coating machine and Frederik Haack for his help with assembling the DAQ system. The authors thank the DLR Energy branch for funding this activity.

REFERENCES

(1) International Energy Agency. *IEA (2020), Cooling, IEA, Paris*. https://www.iea.org/reports/cooling (accessed 2020-11-19).

(2) IRENA. *Heating & Cooling*. https://www.irena.org/heatingcooling (accessed 2020-12-02).

(3) Salamanca, F.; Georgescu, M.; Mahalov, A.; Moustaoui, M.; Wang, M. Anthropogenic Heating of the Urban Environment due to Air Conditioning. *J. Geophys. Res. Atmos.* **2014**, *119* (10), 5949–5965. DOI: 10.1002/2013JD021225.

(4) Lundgren, K.; Kjellstrom, T. Sustainability Challenges from Climate Change and Air Conditioning Use in Urban Areas. *Sustainability* **2013**, *5* (7), 3116–3128. DOI: 10.3390/su5073116.

(5) Li, Z.; Chen, Q.; Song, Y.; Zhu, B.; Zhu, J. Fundamentals, Materials, and Applications for Daytime Radiative Cooling. *Adv. Mater. Technol.* **2020**, *6*, 1901007. DOI: 10.1002/admt.201901007.

(6) Zhao, D.; Aili, A.; Zhai, Y.; Xu, S.; Tan, G.; Yin, X.; Yang, R. Radiative Sky Cooling: Fundamental Principles, Materials, and Applications. *Applied Physics Reviews* **2019**, *6* (2), 21306. DOI: 10.1063/1.5087281.

(7) Catalanotti, S.; Cuomo, V.; Piro, G.; Ruggi, D.; Silvestrini, V.; Troise, G. The Radiative Cooling of Selective Surfaces. *Solar Energy* **1975**, *17* (2), 83–89. DOI: 10.1016/0038-092X(75)90062-6.

(8) Bahadori, M. N. Passive Cooling Systems in Iranian Architecture. *Scientific American* **1978**, *238* (2), 144–155.

(9) Mahdavinejad, M.; Javanrudi, K. Assessment of Ancient Fridges: A Sustainable Method to Storage Ice in Hot-Arid Climates. *ACH* **2012**, *4* (2), p133. DOI: 10.5539/ach.v4n2p133.

(10) Sun, X.; Sun, Y.; Zhou, Z.; Alam, M. A.; Bermel, P. Radiative Sky Cooling: Fundamental Physics, Materials, Structures, and Applications. *Nanophotonics* **2017**, *6* (5), 997–1015. DOI: 10.1515/nanoph-2017-0020.

(11) Raman, A. P.; Anoma, M. A.; Zhu, L.; Rephaeli, E.; Fan, S. Passive Radiative Cooling Below Ambient air Temperature under Direct Sunlight. *Nature* **2014**, *515* (7528), 540–544. DOI: 10.1038/nature13883.

(12) Aili, A.; Wei, Z. Y.; Chen, Y. Z.; Zhao, D. L.; Yang, R. G.; Yin, X. B. Selection of Polymers with Functional Groups for Daytime Radiative Cooling. *Materials Today Physics* **2019**, *10*, 100127. DOI: 10.1016/j.mtphys.2019.100127.

(13) Zhou, L.; Song, H.; Liang, J.; Singer, M.; Zhou, M.; Stegenburgs, E.; Zhang, N.; Xu, C.; Ng, T.; Yu, Z.; Ooi, B.; Gan, Q. A Polydimethylsiloxane-coated Metal Structure for All-day Radiative Cooling. *Nat Sustain* **2019**, *2* (8), 718–724. DOI: 10.1038/s41893-019-0348-5.

(14) Zhai, Y.; Ma, Y.; David, S. N.; Zhao, D.; Lou, R.; Tan, G.; Yang, R.; Yin, X. Scalable-manufactured Randomized Glass-Polymer Hybrid Metamaterial for Daytime Radiative Cooling. *Science (New York, N.Y.)* **2017**, *355* (6329), 1062–1066. DOI: 10.1126/science.aai7899.

(15) Kou, J.; Jurado, Z.; Chen, Z.; Fan, S.; Minnich, A. J. Daytime Radiative Cooling Using Near-Black Infrared Emitters. *ACS Photonics* **2017**, *4* (3), 626–630. DOI: 10.1021/acsphotonics.6b00991.

(16) Yang, P.; Chen, C.; Zhang, Z. M. A Dual-layer Structure with record-high Solar Reflectance for Daytime Radiative Cooling. *Solar Energy* **2018**, *169*, 316–324. DOI: 10.1016/j.solener.2018.04.031.

(17) Son, S.; Liu, Y.; Chae, D.; Lee, H. Cross-Linked Porous Polymeric Coating without a Metal-Reflective Layer for Sub-Ambient Radiative Cooling. *ACS applied materials & interfaces* **2020**, *12* (52), 57832–57839. DOI: 10.1021/acsami.0c14792. Published Online: 21-Dec-20.

(18) Zhong, H.; Zhang, P.; Li, Y.; Yang, X.; Zhao, Y.; Wang, Z. Highly Solar-Reflective Structures for Daytime Radiative Cooling under High Humidity. *ACS applied materials &*

interfaces **2020**, *12* (46), 51409–51417. DOI: 10.1021/acsami.0c14075. Published Online: 04-Nov-20.

(19) Zhu, R.; Hu, D.; Chen, Z.; Xu, X.; Zou, Y.; Wang, L.; Gu, Y. Plasmon-Enhanced Infrared Emission Approaching the Theoretical Limit of Radiative Cooling Ability. *Nano letters* **2020.** DOI: 10.1021/acs.nanolett.0c01457.

(20) Mandal, J.; Fu, Y.; Overvig, A. C.; Jia, M.; Sun, K.; Shi, N. N.; Zhou, H.; Xiao, X.; Yu, N.; Yang, Y. Hierarchically Porous Polymer Coatings for Highly Efficient Passive Daytime Radiative Cooling. *Science (New York, N.Y.)* **2018**, *362* (6412), 315–319. DOI: 10.1126/science.aat9513.

(21) Chen, G.; Wang, Y.; Qiu, J.; Cao, J.; Zou, Y.; Wang, S.; Jia, D.; Zhou, Y. Robust Inorganic Daytime Radiative Cooling Coating Based on a Phosphate Geopolymer. *ACS applied materials & interfaces* **2020**, *12* (49), 54963–54971. DOI: 10.1021/acsami.0c15799. Published Online: 23-Nov-20.

(22) Jeon, S.; Son, S.; Lee, S. Y.; Chae, D.; Bae, J. H.; Lee, H.; Oh, S. J. Multifunctional Daytime Radiative Cooling Devices with Simultaneous Light-Emitting and Radiative Cooling Functional Layers. *ACS applied materials & interfaces* **2020**, *12* (49), 54763–54772. DOI: 10.1021/acsami.0c16241. Published Online: 30-Nov-20.

(23) Tian, Y.; Qian, L.; Liu, X.; Ghanekar, A.; Xiao, G.; Zheng, Y. Highly Effective Photon-to-Cooling Thermal Device. *Scientific reports* **2019**, *9* (1), 19317. DOI: 10.1038/s41598-019-55546-4.

(24) Rephaeli, E.; Raman, A.; Fan, S. Ultrabroadband Photonic Structures to Achieve High-performance Daytime Radiative Cooling. *Nano letters* **2013**, *13* (4), 1457–1461. DOI: 10.1021/nl4004283.

(25) Jaramillo-Fernandez, J.; Whitworth, G. L.; Pariente, J. A.; Blanco, A.; Garcia, P. D.; Lopez, C.; Sotomayor-Torres, C. M. A Self-Assembled 2D Thermofunctional Material for Radiative Cooling. *Small (Weinheim an der Bergstrasse, Germany)* **2019**, e1905290. DOI: 10.1002/smll.201905290.

(26) Zhao, B.; Hu, M.; Ao, X.; Chen, N.; Pei, G. Radiative cooling: A Review of Fundamentals, Materials, Applications, and Prospects. *Applied Energy* **2019**, *236*, 489–513. DOI: 10.1016/j.apenergy.2018.12.018.

(27) Ma, H.; Yao, K.; Dou, S.; Xiao, M.; Dai, M.; Wang, L.; Zhao, H.; Zhao, J.; Li, Y.; Zhan, Y. Multilayered SiO2/Si3N4 Photonic Emitter to Achieve High-performance All-day Radiative Cooling. *Solar Energy Materials and Solar Cells* **2020**, *212*, 110584. DOI: 10.1016/j.solmat.2020.110584.

(28) Chae, D.; Kim, M.; Jung, P.-H.; Son, S.; Seo, J.; Liu, Y.; Lee, B. J.; Lee, H. Spectrally Selective Inorganic-Based Multilayer Emitter for Daytime Radiative Cooling. *ACS applied materials & interfaces* **2020**, *12* (7), 8073–8081. DOI: 10.1021/acsami.9b16742.

(29) Kecebas, M. A.; Menguc, M. P.; Kosar, A.; Sendur, K. Spectrally Selective Filter Design for Passive Radiative Cooling. *J. Opt. Soc. Am. B* **2020**, *37* (4), 1173. DOI: 10.1364/JOSAB.384181.

(30) Li, D.; Liu, X.; Li, W.; Lin, Z.; Zhu, B.; Li, Z.; Li, J.; Li, B.; Fan, S.; Xie, J.; Zhu, J. Scalable and Hierarchically Designed Polymer Film as a Selective Thermal Emitter for High-Performance All-day Radiative Cooling. *Nature nanotechnology* **2020.** DOI: 10.1038/s41565-020-00800-4.

(31) Song, J.; Seo, J.; Han, J.; Lee, J.; Lee, B. J. Ultrahigh Emissivity of Grating-Patterned PDMS Film from 8 to 13 μ m Wavelength Regime. *Appl. Phys. Lett.* **2020**, *117* (9), 94101. DOI: 10.1063/5.0017838.

(32) Heo, S.-Y.; Lee, G. J.; Kim, D. H.; Kim, Y. J.; Ishii, S.; Kim, M. S.; Seok, T. J.; Lee, B. J.; Lee, H.; Song, Y. M. A Janus Emitter for Passive Heat Release from Enclosures. *Science advances* **2020**, *6* (36). DOI: 10.1126/sciadv.abb1906. Published Online: Sep. 4, 2020.

(33) Atiganyanun, S.; Plumley, J. B.; Han, S. J.; Hsu, K.; Cytrynbaum, J.; Peng, T. L.; Han, S. M.; Han, S. E. Effective Radiative Cooling by Paint-Format Microsphere-Based Photonic Random Media. *ACS Photonics* **2018**, *5* (4), 1181–1187. DOI: 10.1021/acsphotonics.7b01492.

(34) Yang Li, Chongjia Lin, Jingyuan Huang, Cheng Chi, and Baoling Huang*. Spectrally Selective Absorbers/Emitters for Solar Steam Generation and Radiative Cooling-Enabled Atmospheric Water Harvesting. *Global Challenges* **2020**, *20.* DOI: 10.1002/gch2.202000058.

(35) Barroso, G.; Li, Q.; Bordia, R. K.; Motz, G. Polymeric and Ceramic Silicon-based Coatings-A Review. *Journal of Materials Chemistry A* **2019**, *7* (5), 1936–1963. DOI: 10.1039/c8ta09054h.

(36) Colombo, P.; Mera, G.; Riedel, R.; Sorarù, G. D. Polymer-Derived Ceramics: 40 Years of Research and Innovation in Advanced Ceramics. *Journal of the American Ceramic Society* **2010**, *73* ([9]), 1805-1837. DOI: 10.1111/j.1551-2916.2010.03876.x.

(37) Banik, U.; Sasaki, K.; Reininghaus, N.; Gehrke, K.; Vehse, M.; Sznajder, M.; Sproewitz, T.; Agert, C. Enhancing Passive Radiative Cooling Properties of Flexible CIGS Solar Cells for Space Applications using Single Layer Silicon Oxycarbonitride Films. *Solar Energy Materials and Solar Cells* **2020**, *209*, 110456. DOI: 10.1016/j.solmat.2020.110456.

(38) Pscherer, M.; Günthner, M.; Kaufmann, C. A.; Rahm, A.; Motz, G. Thin-film Silazane/alumina High Emissivity Double Layer Coatings for Flexible Cu(In,Ga)Se 2 Solar Cells. *Solar Energy Materials and Solar Cells* **2015**, *132*, 296–302. DOI: 10.1016/j.solmat.2014.09.015.

(39) Günthner, M.; Pscherer, M.; Kaufmann, C.; Motz, G. High Emissivity Coatings based on Polysilazanes for Flexible Cu(In,Ga)Se2 Thin-film Solar Cells. *Solar Energy Materials and Solar Cells* **2014**, *123*, 97–103. DOI: 10.1016/j.solmat.2014.01.027.

(40) Li, Y. L., Riedel, R., Steiger, J., & von Seggern, H. Novel Transparent Polysilazane Glass: Synthesis and Properties. *Advanced Engineering Materials* **2000**, *2*, 290–293.

(41) Channa, I. A.; Distler, A.; Zaiser, M.; Brabec, C. J.; Egelhaaf, H.-J. Thin Film Encapsulation of Organic Solar Cells by Direct Deposition of Polysilazanes from Solution. *Adv. Energy Mater.* **2019**, *362*, 1900598. DOI: 10.1002/aenm.201900598.

(42) Banik, U.; Reininghaus, N.; Seefeldt, P.; Sznajder, M.; Gehrke, K.; Vehse, M.; Spietz, P.; Sproewitz, T.; Agert, C. Assessment of Protective Coatings on Flexible CIGS Modules for Satellites. *2019 European Space Power Conference (ESPC)* **2019.** DOI: 10.1109/ESPC.2019.8932031.

(43) Barroso, G.; Döring, M.; Horcher, A.; Kienzle, A.; Motz, G. Polysilazane-Based Coatings with Anti-Adherent Properties for Easy Release of Plastics and Composites from Metal Molds. *Adv. Mater. Interfaces* **2020**, *86*, 1901952. DOI: 10.1002/admi.201901952.

(44) Günthner, M.; Wang, K.; Bordia, R. K.; Motz, G. Conversion Behaviour and Resulting Mechanical Properties of Polysilazane-based Coatings. *Journal of the European Ceramic Society* **2012**, *32* (9), 1883–1892. DOI: 10.1016/j.jeurceramsoc.2011.09.005.

(45) Furtat, P.; Lenz-Leite, M.; Ionescu, E.; Machado, R. A. F.; Motz, G. Synthesis of Fluorine-modified Polysilazanes via Si–H Bond Activation and their Application as Protective Hydrophobic Coatings. *J. Mater. Chem. A* **2017**, *5* (48), 25509–25521. DOI: 10.1039/C7TA07687H.

(46) Lord, S. D. Nasa Technical Memorandum 103957. *Ames Research Center, Moffett Field, CA* **1992**.

(47) Rossi, S.; Deflorian, F.; Fedel, M. Polysilazane-based Coatings: Corrosion Protection and Anti-graffiti Properties. *Surface Engineering* **2019**, *35* (4), 343–350. DOI: 10.1080/02670844.2018.1465748.

(48) Liu, J.; Zhang, J.; Zhang, D.; Jiao, S.; Xing, J.; Tang, H.; Zhang, Y.; Li, S.; Zhou, Z.; Zuo, J. Sub-ambient radiative cooling with wind cover. *Renewable and Sustainable Energy Reviews* **2020**, *130*, 109935. DOI: 10.1016/j.rser.2020.109935.

(49) Chen, Z.; Zhu, L.; Raman, A.; Fan, S. Radiative Cooling to Deep Sub-freezing Temperatures through a 24-h Day-night Cycle. *Nature communications* **2016**, *7*, 13729. DOI: 10.1038/ncomms13729.

(50) Palik, E. D., Ed. *Handbook of Optical Constants of Solids*; Acad. Press, 1997.

(51) Kim; Garland; Abad; Raccah. Modeling the Optical Dielectric Function of Semiconductors: Extension of the Critical-point Parabolic-band Approximation. *Physical review. B, Condensed matter* **1992**, *45* (20), 11749–11767. DOI: 10.1103/PhysRevB.45.11749.

(52) Varner, J. F.; Eldabagh, N.; Volta, D.; Eldabagh, R.; Foley, J. J. WPTherml: A Python Package for the Design of Materials for Harnessing Heat. *Journal of Open Research Software* **2019**, *7*, 100. DOI: 10.5334/jors.271.

Table of Contents

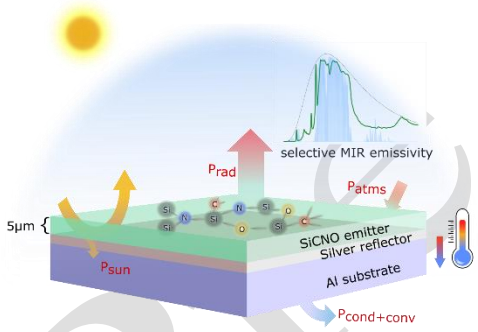

Supporting Information

Efficient Thin Polymer Coating as a Selective Thermal Emitter for Passive Daytime Radiative Cooling

Udayan Banik, Ashutosh Agrawal†, Hosni Meddeb, Oleg Sergeev, Nies Reininghaus, Maximilian Götz-Köhler, Kai Gehrke, Jonas Stührenberg, Martin Vehse, Maciej Sznajder§ζ, Carsten Agert.*

DLR Institute of Networked Energy Systems, 26129 Oldenburg, Germany

§ DLR Institute of Space Systems, 28359 Bremen, Germany

ζ University of Bremen, MAPEX Center for Materials and Processes, 28359 Bremen, Germany

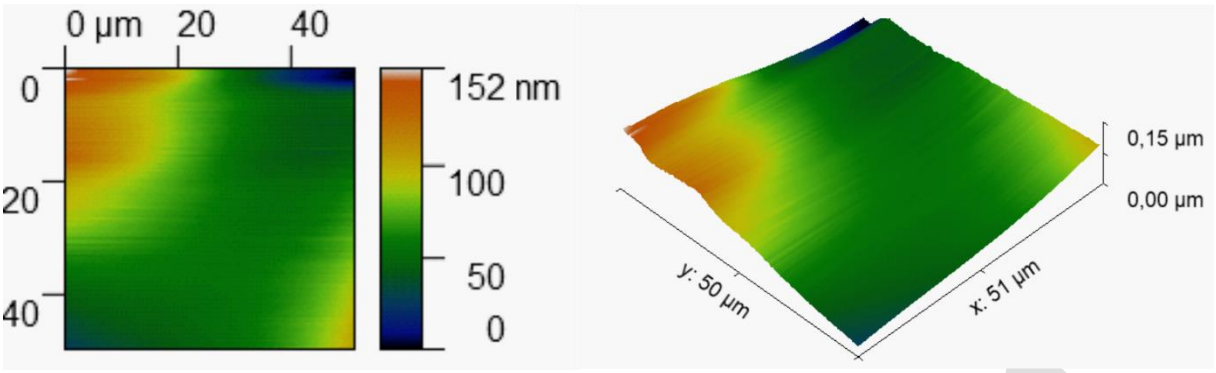

Figure S1. AFM image from a 50 µm x 50 µm area showing the planar morphology of the emitter surface. The RMS surface roughness was calculated to be 22.8 nm.

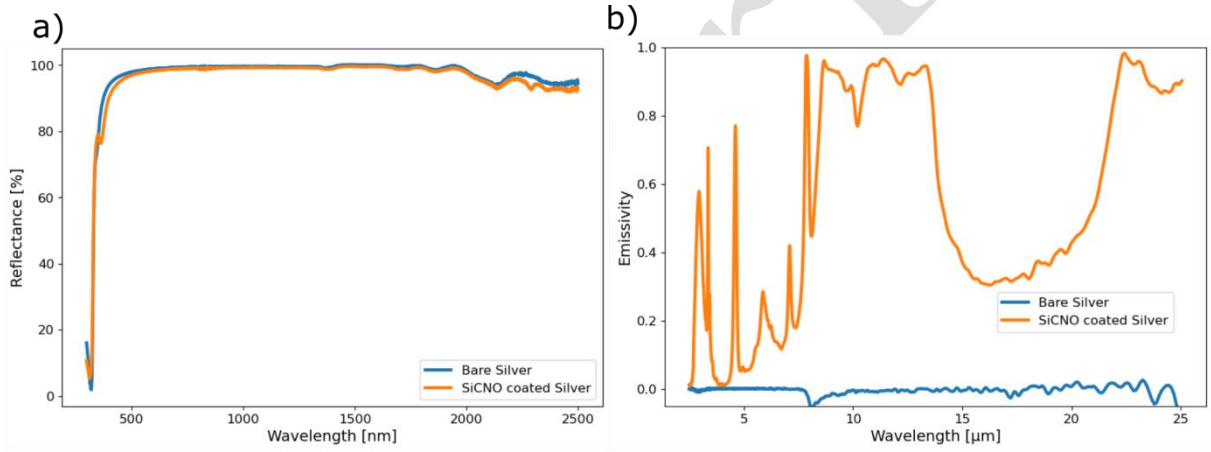

Figure S2. Absorption of light by the SiCNO coating compared to bare silver. a) Reflection spectra comparison of 233nm bare silver with a 5 µm SiCNO coated on silver structure. Under AM1.5 the value of Psun was calculated to be 22.31 Wm-2 whereas with the SiCNO coating it increases to 30.7 Wm-2. b) Emissivity of silver as compared to the SiCNO coated silver structure (same as Figure 2). At some wavelengths the bare silver sample had higher reflection than the gold standard causing emissivity to be slightly below zero.

Supplementary Text S1. Description of equations governing the radiative cooling performance

The absorbed power by the structure due to incident solar irradiation can be calculated as:

$$P_{sun}=A\int_0^{\infty} I_{AM1.5}(\lambda)\,\varepsilon(\lambda,\theta_{sun})d\lambda \quad (1)$$

Where $I_{AM1.5}(\lambda)$ is the reference solar irradiance AM1.5G and $\varepsilon(\lambda,\theta_{sun})$ is the absorptivity in the solar spectrum, since spectral emissivity and absorptivity are equal according to Kirchhoff's Law. Solving Equation (1 using the measured reflection spectra shown in Figure S2a, P_{sun} was calculated to be 30.7 Wm^{-2} for the radiative cooler stack under full AM1.5 radiation. For the rooftop experiment the structure is expected to have lower P_{sun} since the peak solar irradiation was 761.9 Wm^{-2}. The radiative power throughput from the PDRC structure can be calculated using the below equation:

$$P_{rad}(T_{cooler})=A2\pi\int_0^{\frac{\pi}{2}}\int_0^{\infty} I_{BB}(T,\lambda)\,\varepsilon(\lambda,\theta)\sin(\theta)\cos(\theta)d\lambda d\theta \quad (2)$$

Where $I_{BB}(T,\lambda)$ is the spectral irradiance of a blackbody at temperature T, $\varepsilon(\lambda,\theta)$ is the angular spectral emissivity, A is the area of the structure and θ is the zenith angle. Using the angular emissivity spectra from the structure, P_{rad} was calculated to be 194.5 $W.m^{-2}$ at 300K. The impact of the atmosphere on the sample and the absorbed power by the sample due to the atmospheric downward IR radiation can be further understood from the following equation:

$$P_{atm}(T_{amb}) =A2\pi\int_0^{\frac{\pi}{2}}\sin(\theta)\cos(\theta)d\theta\int_0^{\infty} I_{BB}(T_{amb},\lambda)\,\varepsilon(\lambda,\theta)\varepsilon_{atm}(\lambda,\theta)d\lambda \quad (3)$$

Where T_{amb} is the ambient temperature, $\varepsilon_{atm}(\lambda,\theta)$ is the angle dependent emissivity of the atmosphere which is determined by $\varepsilon_{atm}(\lambda,\theta) =1- t(\lambda)^{\frac{1}{cos\theta}}$, where $t(\lambda)$ is the atmospheric transmittance in the zenith. Considering the temperature of the atmosphere and the structure to be 300K and utilizing the angular emissivity, P_{atm} was calculated to be 103.6 $W.m^{-2}$ by solving

Equation (3. The parasitic losses due to conduction and convection can be estimated with the below equation:

$$P_{cond+conv}=A\ h_c(T_{ambient}-T_{sample}) \quad (4)$$

Where h_c is the lumped thermal co-efficient for the parasitic non-radiative contribution due to the temperature difference between ambient and the PDRC structure.

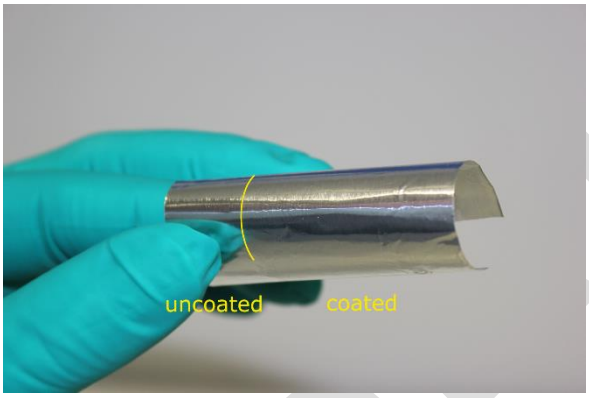

Figure S3 Picture showing the flexible coating property of the PSZ coating. A 5 cm x 5 cm piece of Aluminum foil was coated with PSZ. The coated and uncoated part of the sample is illustrated with a yellow line as it is only visible under close inspection due to high transparency of the coating. The sample was bent around a bending diameter of 15 mm without any observable cracks or spalling of the coating.

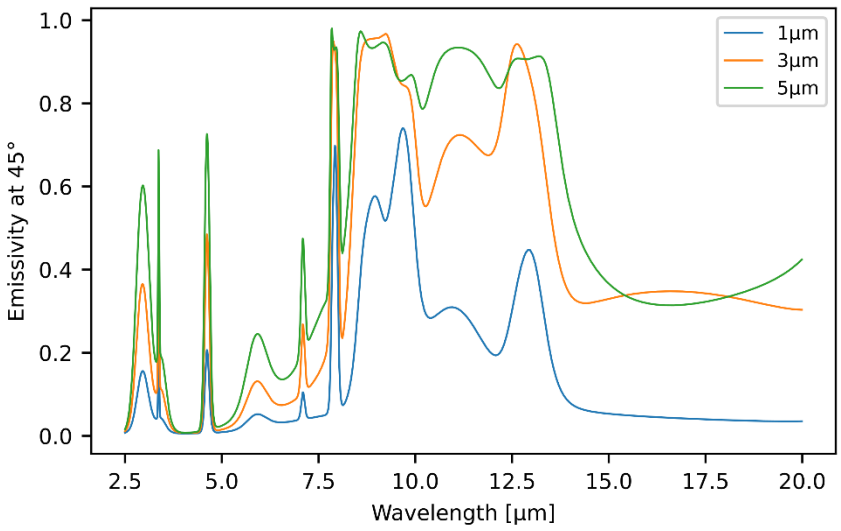

Figure S4 Modelled emissivity (at 45°) spectra of the PDRC device based on thickness variation.

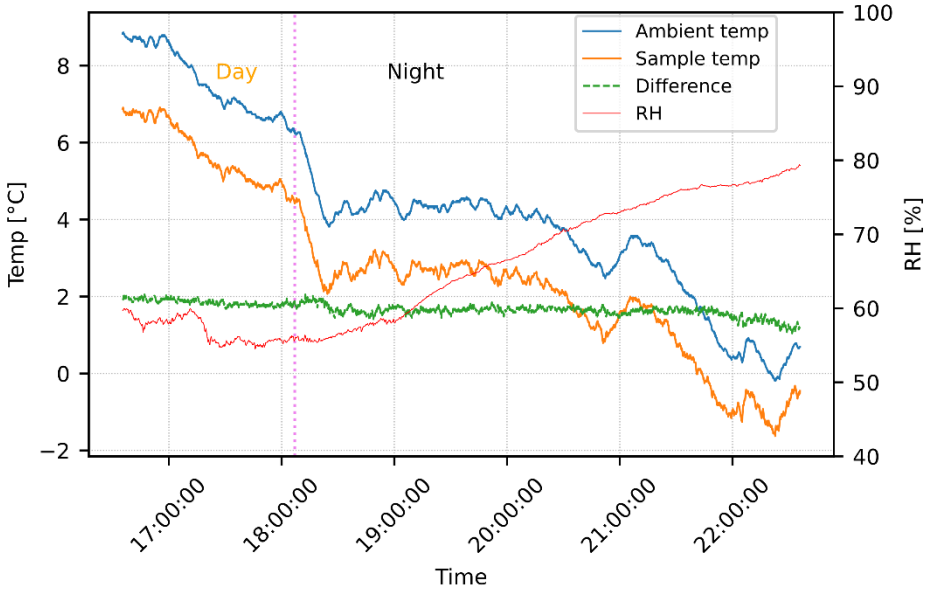

Figure S5 Outdoor temperature measurement of the sample during a winter night (02-03-2021). The experiment was done with the same sample and in the same location as mentioned in the manuscript. Sunset was recorded at 18:07 hrs. (local time), after which a steep drop of the ambient temperature can be observed. The sample temperature reached to 0 °C when ambient was 2 °C. During the measurement time the sample was ~2°C cooler than ambient under humid conditions.